C. R. Mecanique 344 (2016) 267–283

Contents lists available at ScienceDirect

Comptes Rendus Mecanique

www.sciencedirect.com

Computational simulation of manufacturing processes

A methodology to mesh mesoscopic representative volume element of 3D interlock woven composites impregnated with resin

Manh Hung Ha, Ludovic Cauvin, Alain Rassineux *

Sorbonne universités, Université de technologie de Compiègne, CNRS, Laboratoire Roberval, UMR 7337 CNRS/UTC 7337, Centre de recherches de Royallieu, BP 20529, 60205 Compiègne, France

A R T I C L E I N F O

Article history:
Received 8 July 2015
Accepted 29 September 2015
Available online 23 February 2016

Keywords:
Woven composites
Mesh generation
Representative Volume Element
Mesoscopic approach

A B S T R A C T

We present a new numerical methodology to build a Representative Volume Element (RVE) of a wide range of 3D woven composites in order to determine the mechanical behavior of the fabric unit cell by a mesoscopic approach based on a 3D finite element analysis. Emphasis is put on the numerous difficulties of creating a mesh of these highly complex weaves embedded in a resin. A conforming mesh at the numerous interfaces between yarns is created by a multi-quadtree adaptation technique, which makes it possible thereafter to build an unstructured 3D mesh of the resin with tetrahedral elements. The technique is not linked with any specific tool, but can be carried out with the use of any 2D and 3D robust mesh generators.

1. Introduction

In addition to experimental approaches widely used [1–7] to identify the mechanical behavior of composite materials with woven fibrous reinforcement and polymer matrix, numerical simulations can be carried out at a much lower cost. A 3D finite element model of the fabric cell, also denoted as Representative Volume Element (RVE in the text) is first built and this computational unit cell is submitted to different loads. The mechanical behavior can be derived from the results of the analysis and the homogenized properties used at the scale of the structure. The crossing warp yarns and weft yarns in three directions which give to the resulting composite a high structural potential authorize an important number of architectures. With the use of a numerical model, a much wider range of woven structures can be indeed investigated. Once a numerical model is available, the composite properties can be optimized with respect to geometrical or material parameters such as fiber and matrix materials altogether with yarn size and type, yarn placement, yarn paths. New weave types of interlacing yarns can be tested. The approach must be automatic and robust in order to create a high number of RVE, which may be needed to create optimization data. One of the difficulties of a meso–macro approach [8–12] in this context is to reproduce faithfully the geometry of these architectures with complex forms. Studies [9,10] have shown that the definition of the geometry including volume fraction together with the repartition of voids has an important impact on the mechanical properties of the final composite material. One of the main issues in this context is to provide an accurate and realistic contact surface between yarns while avoiding any interpenetration. The textile preform is a porous material

* Corresponding author.
E-mail address: alain.rassineux@utc.fr (A. Rassineux).

http://dx.doi.org/10.1016/j.crme.2015.09.008

composed of thousands of fibers, which are thereafter impregnated with resin. 3D images such as tomography [9,13] shows that this arrangement of fibers inside a yarn is far from being perfect. Fibers can be twisted or entangled. From a mesoscopic scale, the surface of the yarn is the envelope of all its fibers. At this scale, we can consider that the yarn surface is defined by a number of planar cross sections swept along a middle curve denoted as spine. The variation of the volume fraction of fibers and therefore of the local properties of the cell is linked to the changes in the cross section. Therefore, modeling (including geometry and meshing) techniques should take into account contacts between yarns together with local variation of the shape of the cross section due to the reorganization of fibers inside the yarn [9]. Some approaches such as the multifill one [14] propose to simulate the behavior of the woven composite at the scale of the fiber, taking into account the contact at the lower scale of the fiber considered as a beam. Indeed, even if realistic and efficient, the computational time may be prohibitive if the number of fibers (thousands) together with the number of contacts become important. At a higher scale, mesoscopic approaches make use of a finite element analysis to define the mechanical properties of this complex interlacement of yarns. Assumption is made that the yarns composed of a large number of fibers is a homogeneous material, however anisotropic. A great number of yarns (hundreds) can be taken into account at a reasonable computational cost. A number of solutions [8–12,15–17] have been proposed to create a geometry for these complex structures. The mesoscale geometry must be indeed meshed thereafter and this constraint is rarely taken as a priority in the definition of the geometry. The problem of defining an accurate interface is already complex when dealing with dry fabrics only [9]. The difficulties of meshing are a lot more increased if resin is added to the model.

Two steps are usually necessary to create the geometry. The first one consists in creating a coding [16–18] to describe the relative positions (above/under) of the yarns into contact. Indeed, the crossing warp yarns and weft yarns in three directions authorize an important number of architectures. However, coding can be greatly simplified when the orientation of the warp yarn sections is constant. The path of the weft yarns is thereafter defined by the position above or below the warp yarn sections. In that case, the interlaced structure of the 3D multilayered weave can be represented in a matrix form. In a second step, a geometrical model is built. Lomov et al. [19] have proposed solutions to build a geometrical model that takes into account the "crimp" of the yarns inside the fabric in order to provide a realistic physical shape of the intersections between yarns denoted as "elastica model". The model is based on the minimization of bending energy. In most cases, models are often built under the assumption that the yarn's cross section has an imposed shape (mostly elliptical) and remains somehow constant. The variations in both shape and size of the cross section of the yarns have indeed a direct effect on the fiber volume fraction. CAD software packages have the ability to create complex-shaped object, manage with accuracy surface to surface intersections and therefore may provide at first sight a solution. However, even if the geometry of a yarn can be easily represented in most CAD environment, a great number of tasks must be performed in order to build automatically a geometry free of intersections. This could be achieved within an advanced programming environment or a customization of the software, and such tools are rarely provided. At last, a major demand is to mesh the geometrical model, which demands a full integration between geometry and analysis and a control of the mesh generators. CAD-based models and techniques have been discussed and used by Wendling et al. [9]. In the context of the simulation of the deformations of dry fabrics, the authors have proposed a 3D automated CAD-based approach to provide 3D hexahedral elements. In a first step, a realistic 3D geometrical model of the unit cell is created. The model ensures an accurate description of contact areas while avoiding any intersections or spurious space between yarns. In addition, an evolution of the cross section along the middle line is allowed. The technique proposed by the authors proved to be efficient in the context of dry fabrics, but cannot be used when resin must be meshed because only an unstructured mesh generation technique with tetrahedron elements is possible. The authors have proposed in addition a classification into four types of contacts that should be taken into account during modeling: weaving, intermediate, longitudinal, and lateral contacts. The interlock fabric is composed of two yarn networks, warp or weft. When yarn density is low, yarns from the same network are assumed to be parallel, free of contact between them. The weaving contact is due to the interlacement of yarns of the two different networks. This contact is generally taken into account by most geometrical models of the literature. When the density of warp yarn is high, the distance between yarns may be smaller than the yarn width, and lateral contact occurs. Longitudinal contact involves top and bottom yarns of the same network (warp or weft). At last, intermediate contact occurs when the spacing between a yarn and its transverse counterpart is not sufficient. Examples of the most encountered (weaving, intermediate and lateral) contacts obtained with the technique we propose are shown in Figs. 1 and 2.

As we mentioned, the yarn is considered as a homogeneous material, but the behavior of the material is determined by the orientation of the fibers [20], which must be determined with accuracy. In a first assumption, strands can be considered as swept surfaces [9]. In order to create a 3D mesh, a structured mesh of the cross section into quadrangles can be performed and then propagated along a middle axis of the strand in order to create a hex-mesh. The creation of hexahedral elements is preferred to that of tetrahedral elements because, in that case, the orientation of the edges of the elements provides the orientation of the material. Issues to determine fiber orientation in the context of unstructured mesh generation will be discussed in this paper.

The main difficulties pointed out by most authors [9,11] when meshing these 3D woven composites are now discussed. When dealing with a mesoscopic approach based on a finite element analysis, the main concern of geometrical, analytical or CAD-based models should be to provide a model that enables robust mesh generation and thereafter an accurate FE analysis. The geometrical model should at least transform all interpenetrations [11] into contact zones. The shape of the volume of resin inside the RVE is extremely complex and at present, only an unstructured tetrahedron mesh generation is possible.

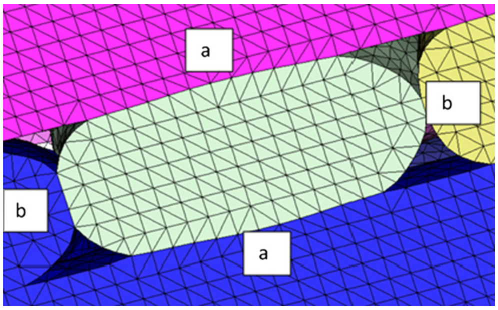

Fig. 1. (a) Weaving contact. (b) Lateral contact.

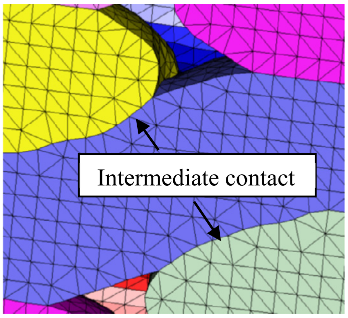

Fig. 2. Intermediate contact.

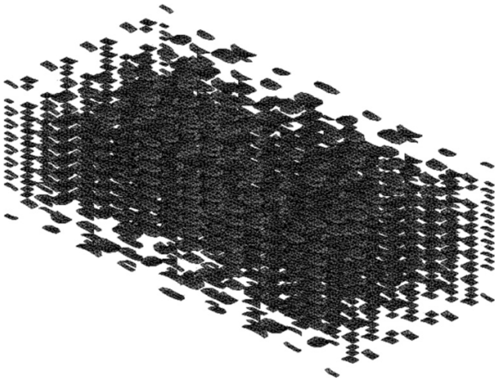

Fig. 3. Numerous contacts at yarn interfaces.

3D unstructured mesh generation can be decomposed into 2 steps. First, a surface mesh of all yarns (one by one) and of the bounding box of the RVE is created. Indeed, the resulting surface mesh must contain no interpenetration, which may surely impede the 3D mesh generation process of the resin. Then 3D unstructured mesh generation [21] can be performed. This second step includes the meshing of all yarns and of the resin, the most complex issue.

As represented in Fig. 3, the number of contact zones can be important (more than 500 on this example for 90 yarns) and the difficulty of meshing is due to the contact between yarns, which requires the same mesh at the interface. In addition, the proximity of opposite yarn faces may impede the convergence of the 3D mesh generator. No spurious space should be added at the interface between yarns. Such space may greatly simplify mesh generation, but as a counterpart may also alter the accuracy of the model [9]. At the interface of two tangent surface yarns, as shown in Fig. 4, flat or elongated elements may be created. In order to avoid this, the smallest element size must be located at the interface between yarns into contacts "around" the contact area where contact between yarns is assumed to be tangent, as illustrated in Figs. 5.

2. Methodology

As we mentioned, creating in a prior approach a geometrical model that avoids unrealistic intersections between stands while taking into account contact areas is an important issue of the whole process. In order to clarify the presentation, a few assumptions are first made on the model. Undulations only occur in the weft direction and not in both weft and

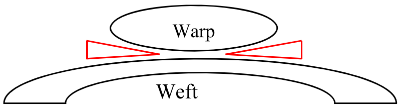

Fig. 4. Location of ill shaped element at the interface of tangent yarns.

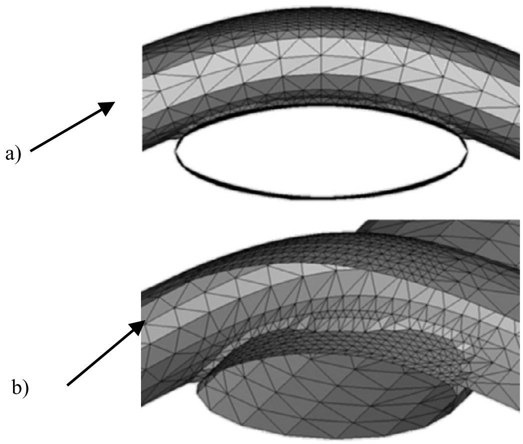

Fig. 5. (a) and (b). Minimal size of element at yarn tangent interfaces.

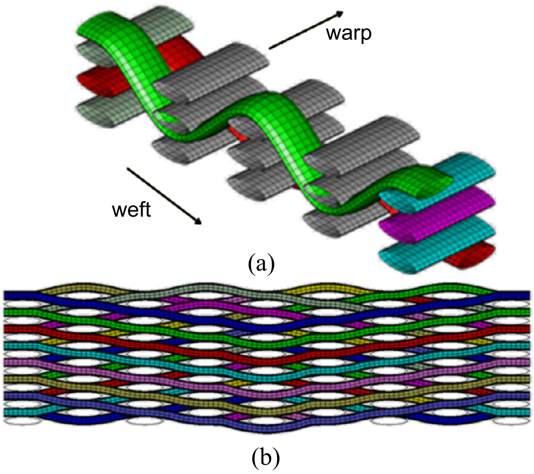

Fig. 6. Weft path across warp yarns. The orientation of the warp yarns is constant.

warp directions, as shown in Figs. 6. In weaving, the weft denotes the yarn that is drawn through the warp yarns to create the material. The undulation of a single weft yarn across warp yarn is represented in Fig. 6(a) and a complex weaving is represented in Fig. 6(b).

The fabric is constituted by a weaving of interlaced yarns at right angles to one another. Cross-sectional areas for both warp and weft are assumed to remain constant and elliptical along a middle axis (straight in the warp direction). The local compression of yarns induced by the process of injection is not taken into account in this first model. At last, we consider that the geometry is ideal and that the trajectory described by the yarns of the same network (warp or weft) remains in parallel planes. The model presented below is built under these assumptions. Both coding and geometry are inspired from WiseTex [15,18]. To our knowledge, among all the techniques proposed to create a mesoscale FE model of multi-dimensional textile composites, no solution to mesh these highly complex 3D structures, including yarn and resin with a conforming mesh at all interfaces, has yet been proposed, even under these simplifying assumptions.

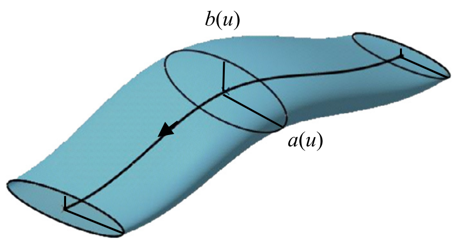

Fig. 7. Variation of elliptical cross-section along the spine in parallel planes.

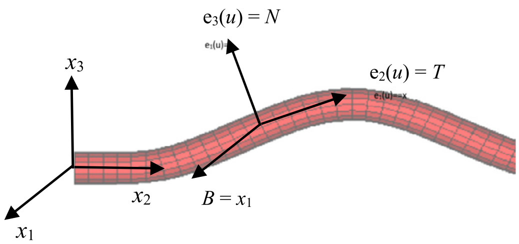

Fig. 8. Orthonormal basis attached to the yarn spine.

2.1. Geometrical model

A number of assumptions are made to build an initial idealized model. The full methodology is presented under these assumptions. However, solutions implemented to make the model more realistic are proposed.

(x_1, x_2, x_3) denotes the global coordinate system in which the RVE is defined. Warp yarn trajectory is first assumed to be a straight line directed by vector x_1. We first consider that each yarn is a surface created by sweeping out an elliptical profile in planes normal to a curve denoted as spine curve. The surface yarn can also be defined by an infinite number of planes normal to a curve denoted as spine. In each plane, the cross section is an ellipse and the center of the ellipse belongs to the spine curve, as shown in Fig. 7. Weft spine curves are therefore contained in planes normal to x_1 (defined in Fig. 8). The orientation of fibers is thereafter provided by the spine curve. The ellipse section is defined by a major radius a and minor radius b along the whole spine and in a plane normal to the spine curve. The yarn surface is therefore fully defined by the control points of the spine and two parameters a and b. If the section varies, but its shape remains elliptical, the two radii $a(u)$ and $b(u)$ may vary along the curve with respect to the curve parameter u, and the yarn surface is a multi-section surface as represented in Fig. 7. We suppose in that case that the information on both radii is given in planes normal to x_1 and x_2 directions for respectively warp and weft yarns, a choice which is compatible with reconstruction techniques based on imaging. Imaging techniques such as X-ray tomography are now widely used for the visualization of the internal structures of an object The resulting cross-sectional images of the object, in our case, the textile geometry, provide information at a high level of precision [9,13]. This process creates a large amount of data (at the scale of the fiber), which must be reduced in order to carry out simulations at the mesoscopic scale of a RVE. The global reconstruction is based on slices taken in parallel planes. Average cross section shapes must be rebuilt. In each plane, segmentation is performed and the contour data of the yarn cross section parameter of the elliptical cross section can be determined at least manually. In practice, the two radii $a(u)$ and $b(u)$ are given at each point of the spine. Between two points, the variation of the parameters is assumed to be linear.

Both models (constant and changing cross section) have been implemented. However, in the scope of this presentation, we consider that the cross section does not change along the spine. Sections are defined in planes normal to the spine and not in parallel planes. The evolution of these planes is given by the unit vectors of Frenet–Serret, tangent vector **T**, the normal vector **N** and the binormal unit vector **B** being the cross product of **T** and **N**. According to our assumptions, weft yarn spine trajectories stay in planes normal to x_1 and the binormal vector is constant and equal to x_1, which means that no torsion is considered and that the curve remains, in a first step, in the osculating plane directed by $(\mathbf{T}, \mathbf{N})$. In the Frenet–Serret frame and under this hypothesis, the curvature κ and the torsion τ of the curve are defined by the following equations:

$$\begin{cases} \frac{\partial T}{\partial s} = \kappa N \\ \frac{\partial N}{\partial s} = -\kappa T + \tau B = -\kappa T \\ \frac{\partial B}{\partial s} = -\tau N = 0 \end{cases} \tag{1}$$

where $s(u)$ represents the arc length along the curve.

The motion of the orthonormal basis $(e_1(u) = x_1, e_2(u), e_3(u))$ attached to the spine is represented in Fig. 8.

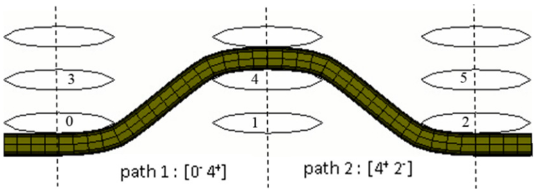

Fig. 9. Weft yarn path coding.

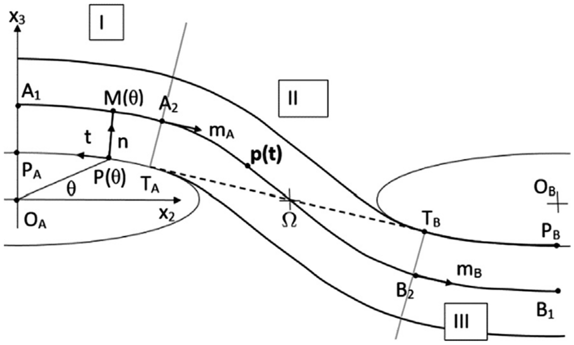

Fig. 10. Weft trajectory on path A^+B^- in plane (x_2, x_3).

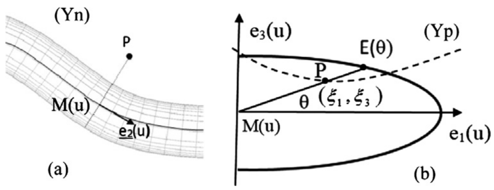

Fig. 11. Relative position of a point P of a yarn Yp with respect to a neighboring yarn surface Yn.

In order to describe the position of weft yarns with respect to warp yarns, a path coding is defined [15]. In our example, we consider that the warp network is composed of elliptical cylinders. The path of the weft yarns is thereafter defined by the position above or below the numbered warp yarn sections. The position below yarn A is defined as A^- and above yarn B, B^+. An example with its corresponding coding is provided in Fig. 9. The whole curve is described by a number of paths between two elliptical half cross sections.

We study all paths between half cross sections A and B: A^-B^-, A^+B^+, A^+B^-, A^-B^+. Among the four possible paths, intersections may only occur on paths A^+B^- and A^-B^+. Let us consider the case A^+B^- represented in Fig. 10. O_A and O_B are the centers of the elliptical warp cross sections in a plane normal to x_1 and containing the spine curve of the weft yarn.

Ω is the middle of O_AO_B, θ is the angle between x_2 and O_AP, P being a point of the warp cross section. T_AT_B is the common tangent line to passing through Ω and below O_B. A_1 is the center of the elliptical cross section of the weft yarn. Curve A_1A_2 (part I in Fig. 10) denotes the offset curve of the part of ellipse between P_A and T_A. Note that the offset of the ellipse is not an ellipse. If $(a_{\text{weft}}, b_{\text{weft}})$ and $(a_{\text{warp}}, b_{\text{warp}})$ denote respectively the two radii of weft and warp yarns, the offset curve is given in Eq. (2) by

$$O_AM(\theta) = O_AP(\theta) + b_{\text{weft}}\frac{n}{\|n\|} \quad \text{with } n = b_{\text{warp}}\cos\theta x_2 + a_{\text{warp}}\sin\theta x_3 \tag{2}$$

where n is a vector collinear to $P(\theta)M(\theta)$ normal to the tangent vector t at point $P(\theta)$ of the ellipse.

The determination of B_2B_1 is similar. Between A_2 and B_2, a cubic Hermite curve $p(t)$ (Eq. (3)) is built. The moduli of vectors $\mathbf{m}_a$ and $\mathbf{m}_b$ can be adjusted in order to control the distance between tangent weft and warp and therefore avoid flat elements.

$$p(t) = \left(2t^3 - 3t^2 + 1\right)A_2 + \left(t^3 - 2t^2 + 1\right)m_A + \left(-2t^3 + 3t^2\right)B_2 + \left(t^3 - t^2\right)m_B \tag{3}$$

This process is repeated with all paths between half warp cross sections. In an ultimate step, all curves are reunified into a single spline curve with a fine discretization. This curve can be considered as the spine of the yarn surface.

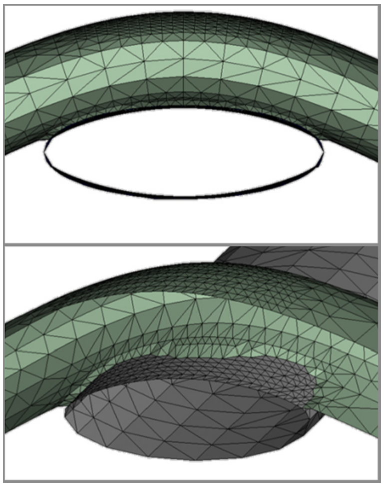

Fig. 12. Offset around the contour of yarn interfaces.

2.2. Detection of intersections and contacts

In order to detect intersections, we need to determine the position of a point of a yarn *Yp* with respect to all neighboring yarns. In Fig. 11(a), a point P belonging to yarn *Yp* is projected on the spine of a neighboring yarn *Yn*. *Yp* is not represented in Fig. 11(a), but is displayed with dotted lines in Fig. 11(b). The projection of P on the spine of yarn *Yn* is $M(u)$. In the plane normal to the spine of *Yn* at point $M(u)$, the cross section is an ellipse represented in Fig. 11(b). The projection $M(u)$ and therefore the parameter u is obtained easily by minimizing criterion $J(u)$ of Eq. (4), where u denotes the parameter along the spine curve and $e_2(u)$ the unit tangent vector to the curve:

$$J_u(P) = \big(PM(u) \cdot e_2(u)\big)^2 \tag{4}$$

Once parameter u together with projection point $M(u)$ have been determined and therefore the plane normal to the curve that contains point P, local coordinates (ξ_1, ξ_2) in the mobile plane $(M(u), e_1(u), e_3(u))$ are calculated as displayed in Fig. 11. If E denotes the radial projection of point M on the ellipse, θ the angle between e_1 and $ME(\theta)$, the condition of intersection can be written as following equation (5).

$$\big\|PM(u)\big\| \le \big\|E(\theta)M(u)\big\| \quad \text{with } \theta = \tan^{-1}\left(\frac{b_{\text{warp}}\xi_1}{a_{\text{warp}}\xi_3}\right) \tag{5}$$

When the point is outside the surface, the shorter distance to the surface yarn (and not the radial distance) is calculated. The goal is to refine the mesh when two surfaces are close. The method is ruled by the position of a point with respect to a planar contour. We have extended the technique to contours described by segments that include varying sections (Fig. 7) and deformed sections as well. The computational cost to determine the position of the point is in that case increased [22].

We propose here a technique to avoid flat elements at the interface contour (Fig. 4) between yarn surfaces in order to ensure the robustness of the meshing process. An offset of all cross sections is first performed. The dimensions of the extended surfaces are increased from a distance which is linked to the chosen smallest mesh size. The relative position of a point with respect to contours is performed with these increased dimensions. If a point P is located inside a contour, the point is positioned at its radial projection E as shown in Fig. 11. Fig. 12 shows that the computation of intersections on the inflated model and the return to the original size provides space outside the contour of yarn interfaces. In addition, in order to control this volume of resin between yarns, a mesh adaptation is proposed in Section 2.3. A high-quality tetrahedron can be thereafter performed while allowing minor changes in the shape at the vicinity of tangent yarn surfaces.

2.3. RVE box

The geometry of the model includes the definition of a RVE which takes into account the periodicity of the fabric cell [23]. In order to reduce the computational time, the ideal choice is to determine the smallest configuration from which the whole fabric can be rebuilt by the use of translations. In order to define the RVE, the mesh is trimmed by four planes normal to directions x_1 and x_2, which can be seen as a rectangular-based cylinder as shown in Fig. 13(a). On this example, no trim has been performed in direction x_3. The result of the trim after remeshing the yarns is shown in Fig. 13(b). The mesh of the yarn is performed is the parameter space and therefore the intersections between the RVE box and the yarn must be determined. A mesh of the yarn in the entire parameter space is performed and element outside the box are eliminated.

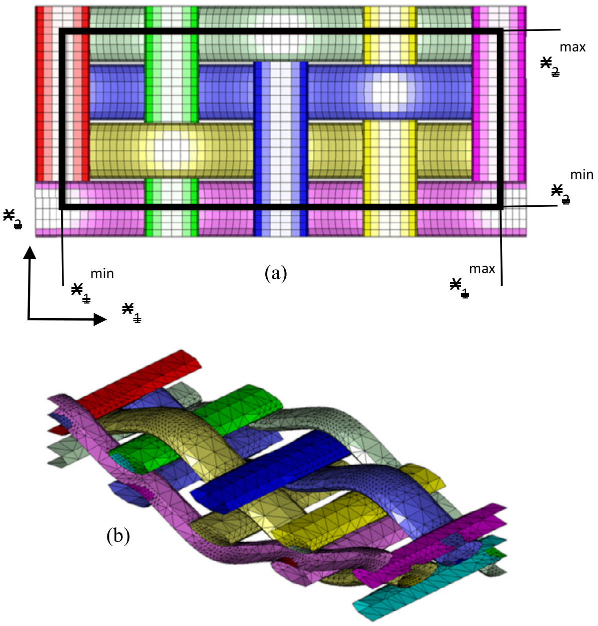

Fig. 13. (a) Definition of a RVE trimmed by 4 planes. (b) Yarns of the RVE are trimmed.

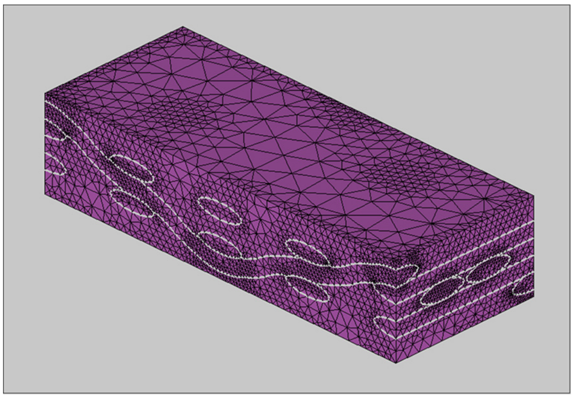

Fig. 14. RVE box.

Some yarn surfaces are intersected by planes of the RVE corresponding to $x_1 = x_1^{\min}$, $x_1 = x_1^{\max}$, and $x_2 = x_2^{\min}$, $x_2 = x_2^{\max}$. If point A_1 represented in Fig. 10 is located in one of these four RVE planes, the geometrical model of a weft yarn spine as presented in Section 2.1 ensures periodical conditions as the tangent vector to the spine curve at A_1 is horizontal. When the shape of the yarn elliptical cross section is flat (ratio between bigger and smaller radius exceeds 5), we experienced that the surface trim in direction x_3 may impede the quality of the final mesh together with the robustness of the 3D meshing process of the resin. In this case, a RVE of the full fabric in direction x_3 has been performed. In all cases, the RVE filled with resin is a box as shown in Fig. 14 on which the frontiers of the yarn surfaces have been represented.

2.4. Meshing issues

The whole mesh process is divided into three steps:

- the mesh of each yarn surface,
- the mesh of the box of the RVE,
- the mesh of the resin.

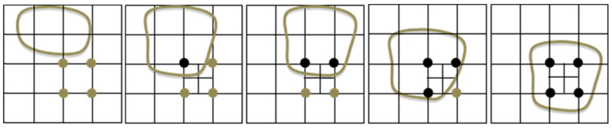

Fig. 15. Multi-quadtree splitting configurations.

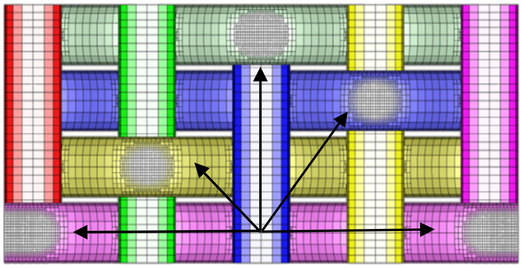

Fig. 16. Adaptation to the proximity of the RVE faces.

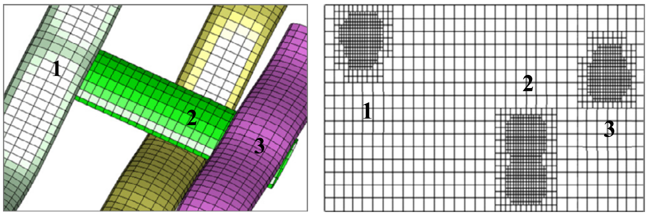

Fig. 17. Quadtree refinement at intersection.

2.4.1. Yarn surface mesh

In this section, yarn surfaces are described as swept surfaces along a spine curve with a constant elliptical cross section. L^e denotes the approximate length of the ellipse and L^s the length of the spine. The yarn surface is considered as developable and can be easily represented in parameter space (U, V) by a rectangular grid where

$$U = L^s \times u, u \text{ denotes the parameter of the spine}$$
$$u \in [0, 1] \quad \text{and} \quad V = L^e \times v \text{ with } v = \frac{\theta}{2\pi}$$

The maximal size of the surface mesh is driven by the discretization of the cross section. The main idea is to start with a coarse mesh of the surface and then to refine in the areas into contact and in the vicinity of a plane of the RVE. To determine the maximal mesh size, a quarter of the elliptical cross section is split into 2, 4 or 2^{ns} segments, where ns is a user fixed parameter. Note that the discretization is not performed with respect to an angle criterion, but that the curve is discretized into segments that have approximate equal length [24]. The maximal size $t_{\max}$ is thereafter given by the length of a segment of the ellipse. Each element of the initial mesh is considered as a quadtree [24,25] and therefore may be split. The number of splitting iterations is given a priori and provides the smallest mesh size. The idea is to divide recursively each cell and the process can be described as a multi-quadtree technique. The only information needed to perform the algorithm is the relative position of a yarn point with respect to another yarn and with respect to the distance to a plane of the RVE. Depending on the position of a point (inside, outside, into contact), the cell is split. The splitting stops when the ultimate level is reached. The splitting algorithm can be described as follows: a cell cannot be split more than ns times.

For each yarn surface and for each cell, if the cell has been split ns time, no operation is performed; otherwise, we locate the number of points inside another yarn. The different configurations encountered are represented in Fig. 15. Inner and contact points are displayed in black.

If the number of inner or contact point is zero, no splitting of the cell is performed. In all other cases, the cell is divided. Adaptation is also driven by the distance to the top and bottom planes of the RVE as can be seen in Fig. 16. At the end of the process, the multi-quadtree is equilibrated, so that the ratio of size of neighboring cells does not exceed 2.

Examples of the multi-quadtree adaptation are shown in Figs. 17 and 18. In Figs. 17, three intersection areas have been detected and numbered in both 3D and parameter spaces.

In Fig. 18, the 3D mesh of an adapted yarn has been represented. The colored cells are located at the contact with other yarns. Note that the mesh has been also refined due to the proximity of the top RVE plane.

Some important remarks and reminders must be made. At first, the detection of intersections is performed on the offset extended geometry. The dividing process is controlled by a single parameter ns and therefore all segments on the intersection contour have the same length. The process is carried out in the space parameter attached to each yarn. Intersection

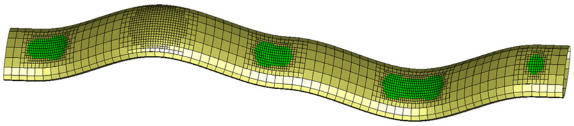

Fig. 18. Quadtree mesh adaptation of a yarn.

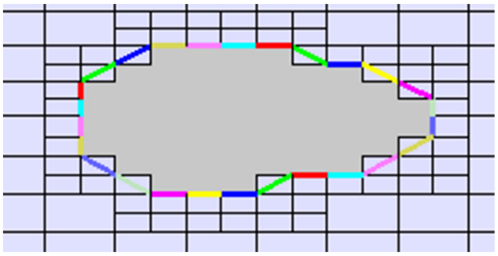

Fig. 19. Smoothing of intersection contours.

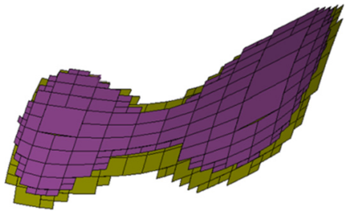

Fig. 20. Intersection contours on both yarns.

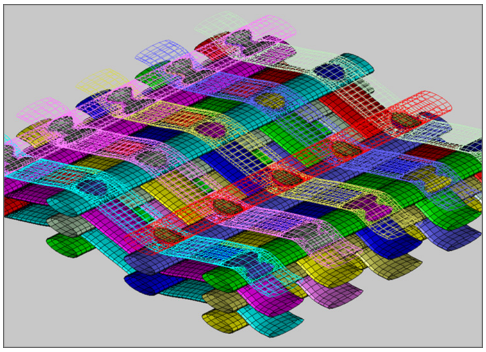

Fig. 21. Multi-quadtree adaptation. A high number of intersections can be handled.

contours must be smoothed in order to eliminate the Manhattan shape, which can be easily obtained by breaking 90° angles without removing any node from the interface, as shown in Fig. 19.

The final surface mesh is indeed performed in the space parameter and includes the outer boundaries and the intersection contours, a point detailed thereafter. Note that the outer boundary can be trimmed by an intersection or by a plane of the RVE. The intersection between yarns S_1 and S_2 can be obtained by analyzing the relative position of points belonging to S_1 with respect to S_2 (noted as $S_1 \cap S_2$) or the relative position of points belonging to S_2 with respect to S_1. As shown in Fig. 19, both 3D intersection are slightly different.

As shown in Fig. 20, the 3D intersection contours $S_1 \cap S_2$ and $S_2 \cap S_1$ are different. In order to create a conforming mesh at the interface between two surfaces, one of them denoted as master surface keeps its intersection nodes, while the other, the slave surface, inherits from the other the whole intersection contour. As the intersection contour of the master surface is close to the slave surface thanks to the adaptation, the master nodes can be easily projected on the slave surface. The projection of the nodes on the slave surface is similar to that in Section 2.2. When a surface inherits a contour from another one, nodes inside or close to the projected contours are removed. The multi-quadtree adaptation technique is very robust and a high number of intersections can be handled at a very low computational time as shown in Fig. 21, in which intersection areas have been represented.

Yarn surfaces cut by the RVE planes must be trimmed in the 2D parameter space. If the yarn surface is trimmed by a plane normal to the spine curve, parameter u along the curve is determined (see Section 2.2) for both intersections. In that

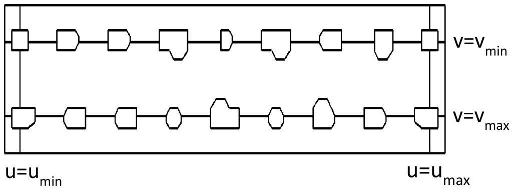

Fig. 22. Yarn surface trimmed by RVE planes in parameter space.

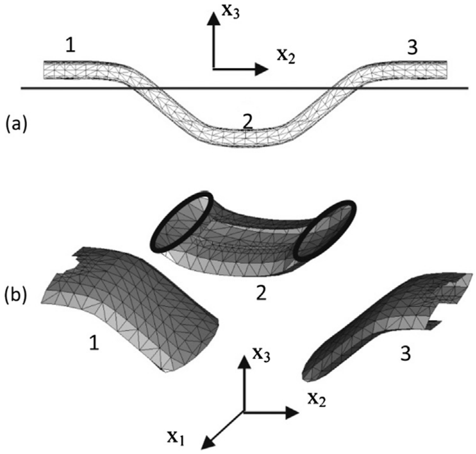

Fig. 23. Yarn surface trimmed in direction x_3. (a) Position of the cutting plane. (b) Position of the three pieces in the RVE.

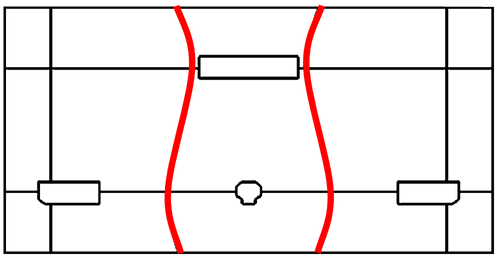

Fig. 24. Representation in parameter space of two closed curves resulting from RVE trim in the x_3 direction.

case, the surface is always trimmed by two parallel planes of the RVE and two parameter values $u_{\min}$ and $u_{\max}$ must be determined. In the other case, the parameter v is 0.25 or 0.75, corresponding to $\theta = 90°$ or -90 on the ellipse. In Fig. 22, the surface yarn is trimmed with respect to both parameters u and v.

If the fabric is trimmed in direction x_3 by an inferior and superior plane, the yarn can be divided in a number of non-adjacent pieces as shown in Figs. 23 where the yarn is cut into three pieces. Fig. 23(a) shows the position of the cutting plane normal to x_3 and Fig. 23(b) the position of the different pieces in the RVE. The position of part 2 under the cutting plane in Fig. 23 has changed to the top of the RVE and we remark that with these different pieces in that position, RVE can be superposed. The two intersection contours (closed curves) between the plane and the second piece in Fig. 23(b) are represented in Fig. 24 in the parameter space. In order to build these curves, we determine each intersection in the parameter space between an iso-v spline and the cutting plane. A cubic spline in the parameter space is created from these points.

Fig. 25 provides an illustration of an interlock RVE denoted as H2 [26] trimmed in the x_3 direction.

Boundary and intersection curves are thereafter discretized with respect to mesh density [24], and a 2D mesh is performed in the parameter space. A 3D surface mesh is created thereafter. We remind the reader that the mesh inside contours resulting from an intersection with a master surface is replaced by the inner mesh of the master surface in order to guarantee a matching mesh at the interfaces.

A surface yarn is represented in Fig. 26(a) and its representation in the space parameter in Fig. 26(b). On this example, the intersection contour with another yarn intersects the iso-curve $v = 0$. Periodicity in the context of surface mesh generation has been widely discussed [27] and the solution consists either of trimming the outer contour as proposed in Fig. 26(b).

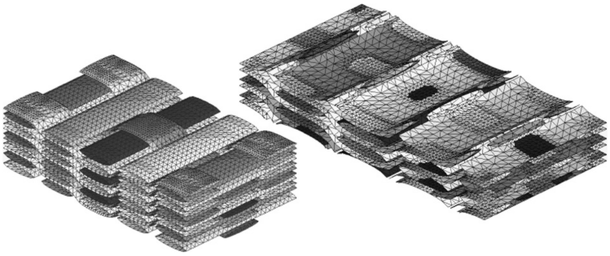

Fig. 25. RVE of H2 interlock trimmed in the x_3 direction.

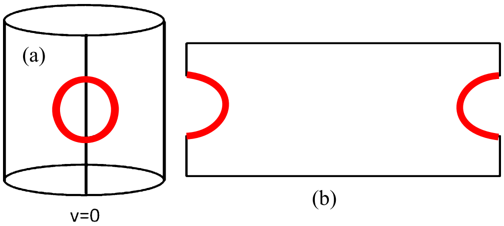

Fig. 26. (a) 3D intersection contour on iso $v = 0$. (b) The outer contour is trimmed in parameter space.

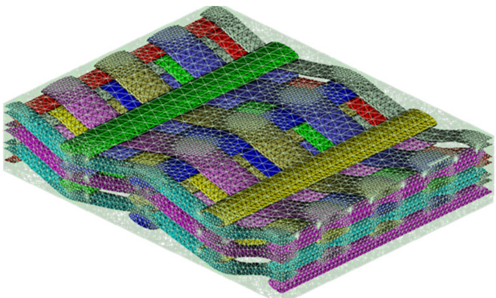

Fig. 27. RVE box. Both yarn mesh and mesh box are represented.

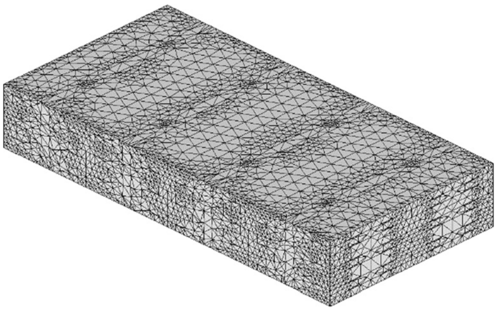

Fig. 28. RVE box of H2 interlock trimmed in the x_3 direction.

Only minor changes have been necessary in order to take into account a model in which cross sections may vary as represented in Fig. 7. The only requirements to carry out this technique are: the definition of a 2D parameter space, the definition of a surface spine, the location of a point with respect to a contour. However, in that case, the volume of information together with the computational time increases with the complexity of the model.

2.4.2. Meshing the RVE box

The adapted surface mesh of all yarns has been processed. As shown in Fig. 14, all edges from this mesh belonging to a RVE plane are identified. The 12 edges of the RVE box are first discretized and a mesh of each RVE faces can be performed. The inner mesh density is given by the size of the inner edges resulting from the trim, but also by the proximity to a surface yarn, as clearly represented in Fig. 27, on which both yarn mesh and box mesh are displayed.

The RVE box of the H2 composite introduced in Fig. 25 is displayed in Fig. 28. The fabric cell is trim along directions x_1, x_2, and x_3.

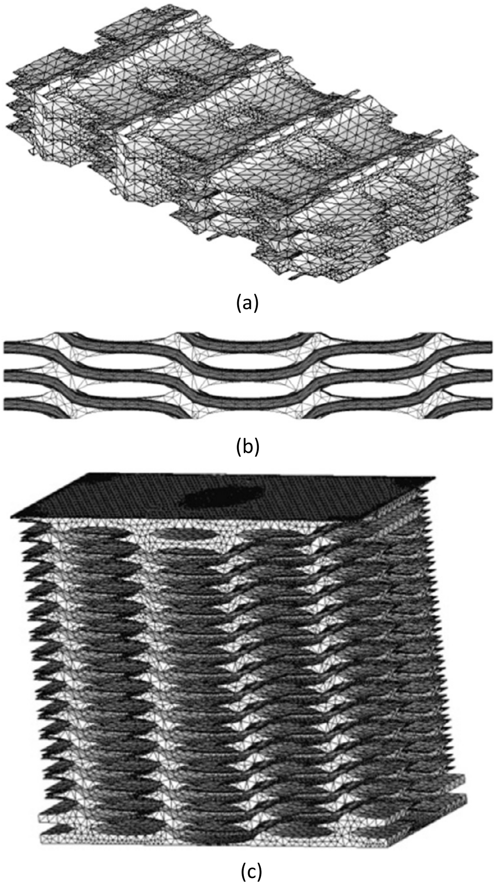

Fig. 29. Resin mesh of H2 interlock: (a) and (b) trimmed in all directions, (c) no trim in the x_3 direction.

2.4.3. Unstructured mesh of the resin and the yarns

Meshing the resin is indeed the ultimate goal of this work and what mostly justifies the numerous necessary steps detailed above. Some yarn surfaces are quite close to one another and when yarn density is high, mesh adaptation is the solution to control the inter-yarn distance and therefore to provide a better respect of the geometry. The outer boundary of the resin composed of yarn surfaces and some areas of the box is created and the 3D mesh can be carried out. The shape quality criterion q chosen to define the shape quality of a tetrahedron T is defined in Eq. (6) as the ratio of the radius r_i of the sphere inscribed in the element to the longest edge length h of the element. A coefficient α is applied so that the criterion of an equilateral element is set at 1.

$$q(T) = \alpha \times \frac{r_i}{h} \tag{6}$$

We experienced that no element had a quality criterion below 0.1, even for the most complex meshes. In Fig. 29, the case displayed is the H2 interlock composite [26] proposed before. Figs. 29(a) and (b) show different views of the resin mesh when a trim in direction x_3 is performed, and Fig. 29(c) the situation when no trim is performed in that direction. The resin mesh is composed of respectively 56,000 nodes and 280,000 elements.

In a final step, all yarns are meshed independently into tetrahedra and all nodes are merged to create a tetrahedron mesh with conforming meshes at the interface of yarns into contacts.

2.5. Fiber orientation

Yarns have an orthotropic behavior and it is therefore essential to determine the orientation of the fibers. When dealing with structured hexahedral meshes created by a 2D planar mesh swept along the spine curve, the orientation can be easily determined. In the case of a tetrahedron mesh, we make the assumption that the orientation of the fibers is provided by the spine curve. If we consider a point inside a yarn, its projection on the spine curve has been detailed in Section 2.2. Once the parameter on the curve has been determined, a tangent vector provides the orientation of the fibers.

For each yarn, we compute the maximum angle amplitude $\Delta\theta$ made between the orientation $\theta = 0$ and the tangent to the spline curve as shown in Fig. 30.

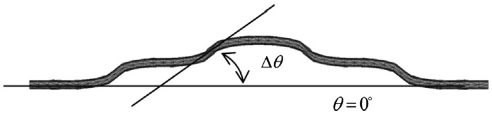

Fig. 30. Assignation of materials with respect to an angular range.

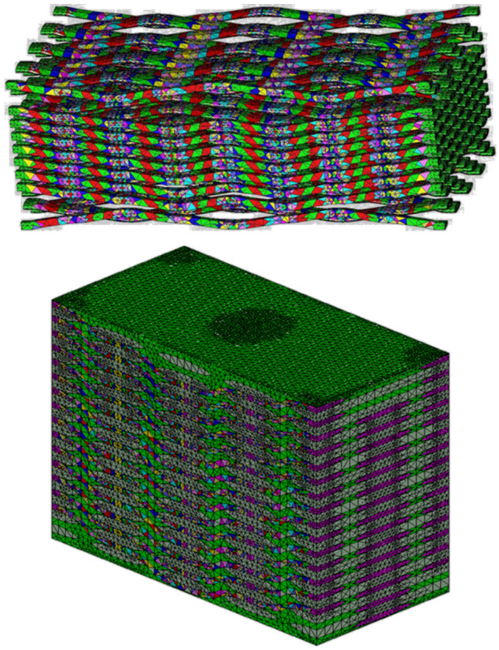

Fig. 31. Determination of fiber orientation.

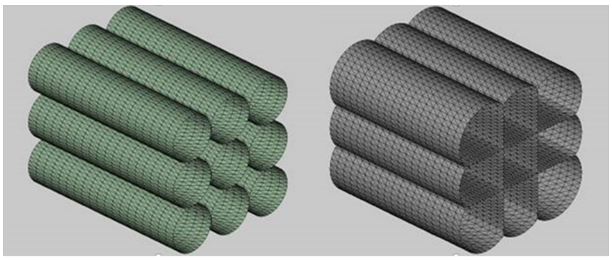

Fig. 32. Inflation process. Nodes are fixed when a contact is detected.

Indeed, the same material is attributed to θ and $-\theta$ oriented fibers. In practice, the number of desired materials m is a parameter chosen a priori. Material i corresponds therefore to an angle between $(i-1)\frac{\Delta\theta}{m}$ and $i\frac{\Delta\theta}{m}$. An illustration is provided in Figs. 31 for two different RVE with and without the resin mesh. A material has been assigned for each angular degree what provides an accurate representation of the fiber orientation.

2.6. Extension of the technique

Many difficulties must be solved in order to create a RVE of these complex structures and therefore we have chosen to present the technique with a number of restrictions:

- undulations only occur in the weft direction,
- the cross section is an ellipse and remains constant,
- the trajectory described by the yarns of the same network remains in parallel planes.

Issues to generalize the technique presented above are now discussed. We suppose that both warp and weft yarns are given by a spine curve represented as a cubic spline. The model is defined as a multi-section surface as represented in Fig. 7. We still suppose that the cross section can be represented by an ellipse and that the information about the cross section radii

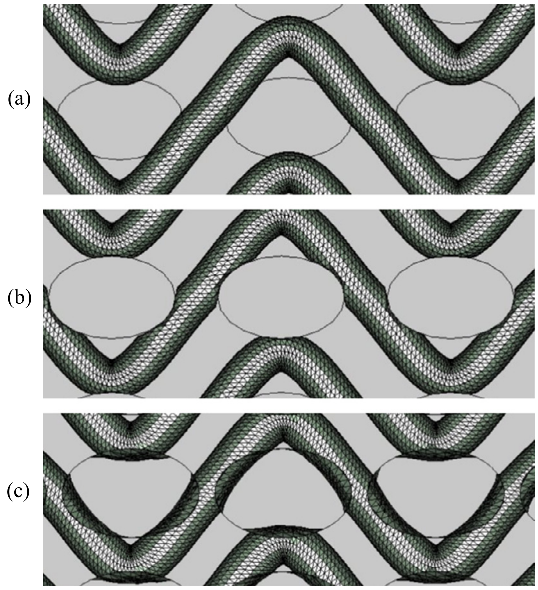

Fig. 33. Detection of contacts: (a) initial model with intersections, (b) contact between fixed warp yarns and weft yarns, (c) deformation between yarns into contact is balanced.

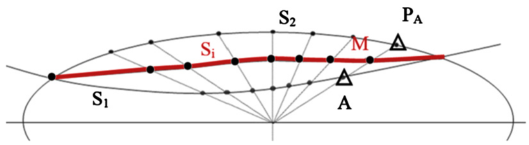

Fig. 34. A radial projection is chosen to determine the mid-surface.

is given in parallel planes and not in planes normal to the spine. The model proposed here is not free of intersections and the method proposed in Section 2 to build a geometrical model is no longer used. The global idea of the technique is to build a first quadrangular mesh grid free of intersections by reducing the radii of all yarns with the same coefficient, for instance 50%. We first determine a threshold at which no intersection occurs. Once again, the only requirement to perform the algorithm is to locate a point inside a contour that has been discussed previously. Then, the model is inflated to its original size while stopping the increase for the nodes in contact. In practice, an increment of 10% has been chosen. The computational time, which could be neglected with the previous technique, increases, but the process still remains efficient (one minute for a hundred yarns for the growing process). The process is first validated with analytical examples and illustrated in Figs. 32 with cylinders. As a result, a planar mesh is created at the intersection areas.

On the following Figs. 33, warp yarns remain straight and parallel while weft yarns undulate. Fig. 33(a) shows a mesh with clear intersections.

In Fig. 33(b), the cross section of waft yarn has been fixed while weft yarn cross sections are allowed to grow. Finally, in Fig. 33(c), the deformation of warp and weft cross sections has been balanced. The large increment of cross section parameters chosen reduces the computational time, but may allow severe intersections. A mid-surface must be created at the interface between yarns. We consider the intersection between yarns S_1 and S_2. A planar representation is provided in Fig. 34 for clarity purposes. S_2 is represented by an ellipse in the figure plane. A denotes a point of surface S_1 which is clearly inside yarn S_2. A radial projection P_A is performed and both points A and P_A are relocated at mid-point M. The process is carried out for each point of surface S_1. Note that a master surface must be chosen.

Figs. 35 provide an illustration of the performance of the technique. Multiple contacts including lateral contact as well as clear variation of cross-sections can be obtained.

3. Conclusion

A methodology to create complex RVE of woven composites embedded in a resin for mesoscale analysis has been presented. Even if the geometry of the fabric is idealized, a great number of difficulties must be solved to create a conforming mesh of these interlaced yarns together with the resin. Issues to extend the idealized geometry to more realistic ones have been proposed. The next step may consists in building such finite element models from the data of 3D images such as X-ray tomography and to compare the model predictions to experimental data.

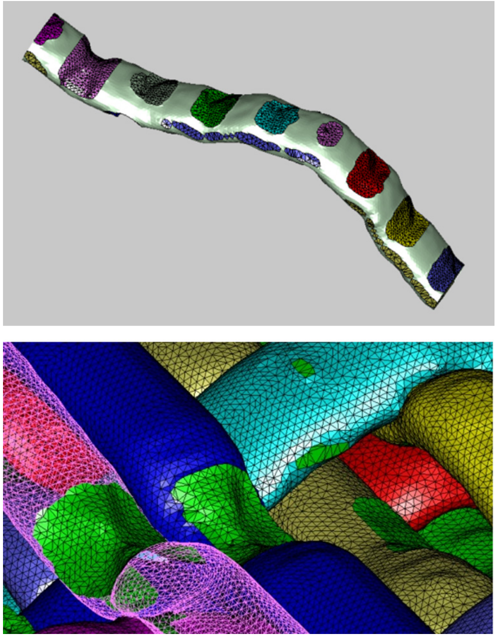

Fig. 35. Multiple contacts and variation of the cross section.

References

[1] B.K. Behera, B.P. Dash, Mechanical behavior of 3D woven composites, Mater. Des. 67 (2015) 261–271.
[2] G. Hivet, A.V. Duong, A contribution to the analysis of the intrinsic shear behaviour of fabrics, J. Compos. Mater. 45 (6) (2011) 695–717.
[3] Z. Aboura, K. Khellil, M.L. Benzeggagh, A. Bouden, R. Ayad, A new generation of 3D composite materials: advantage and disadvantage, in: Damage and Fracture Mechanics: Failure Analysis of Engineering Materials and Structures, 2009, pp. 473–483.
[4] A. Willems, S.V. Lomov, I. Verpoest, D. Vandepitte, Optical strain fields in shear and tensile testing of textile reinforcements, Compos. Sci. Technol. 68 (2008) 807–819.
[5] S.V. Lomov, D.S. Ivanov, T.C. Truong, I. Verpoest, F. Baudry, K. Vanden Bosche, H. Xie, Experimental methodology of study of damage initiation and development in textile composites in uniaxial tensile test, Compos. Sci. Technol. 68 (12) (2008) 2340–2349.
[6] J. Cao, R. Akkerman, P. Boisse, J. Chen, H.S. Cheng, E.F. de Graaf, J.L. Gorczyca, P. Harrison, G. Hivet, J. Launay, W. Lee, L. Liu, S.V. Lomov, A. Long, E. de Luycker, F. Morestin, J. Padvoiskis, X.Q. Peng, J. Sherwood, Tz. Stoilova, X.M. Tao, I. Verpoest, A. Willems, J. Wiggers, T.X. Yu, B. Zhu, Characterization of mechanical behavior of woven fabrics: experimental methods and benchmark results, Composites, Part A, Appl. Sci. Manuf. 39 (6) (2008) 1037–1053.
[7] A. Gasser, P. Boisse, S. Hanklar, Analysis of the mechanical behaviour of dry fabric reinforcements. 3D simulations versus biaxial tests, Comput. Mater. Sci. 17 (1) (2000) 7–20.
[8] S.V. Lomov, I. Verpoest, Model of shear of woven fabric and parametric description of shear resistance of glass woven reinforcements, Compos. Sci. Technol. 66 (7–8) (2006) 919–933.
[9] A. Wendling, G. Hivet, E. Vidal-Sallé, P. Boisse, Consistent geometrical modelling of interlock fabrics, in: 90 Finite Elements in Analysis and Design, 2014, pp. 93–105.
[10] P. Badel, E. Vidal-Sallé, E. Maire, P. Boisse, Simulation and tomography analysis of textile composite reinforcement deformation at the mesoscopic scale, Compos. Sci. Technol. 68 (2008) 2433–2440.
[11] S.V. Lomov, D.S. Ivanov, I. Verpoest, M. Zako, T. Kurashiki, H. Nakai, S. Hirosawa, Meso-FE modelling of textile composites: road map, data flow and algorithms, Compos. Sci. Technol. 67 (9) (2007) 1870–1891.
[12] S.V. Lomov, Virtual testing for material formability, in: A. Long (Ed.), Composite Forming Technologies, Woodhead, Cambridge, 2007, pp. 80–116.
[13] Renaud G. Rinaldi, Matthew Blacklock, Hrishikesh Bale, Matthew R. Begley, Brian N. Cox, Generating virtual textile composite specimens using statistical data from micro-computed tomography: 3D tow representations, J. Mech. Phys. Solids 60 (8) (2012) 1561–1581.
[14] D. Durville, Simulation of the mechanical behaviour of woven fabrics at the scale of fibers, Int. J. Mater. Form. 3 (2) (2010) 1241–1251.
[15] I. Verpoest, S.V. Lomov, Virtual textile composites software WiseTex: integration with micro-mechanical, permeability and structural analysis, Compos. Sci. Technol. 65 (15–16 spec. iss.) (2005) 2563–2574.
[16] S.V. Lomov, G. Huysmans, I. Verpoest, Hierarchy of textile structures and architecture of fabric geometric models, Tex. Res. J. 71 (6) (2001) 534–543.
[17] M. Sherburn, Texgen open source project, http://texgen.sourceforge.net/index.php/main_page.
[18] Wisetex, http://www.mtm.kuleuven.be/onderzoek/composites/software/wisetexis#.
[19] S.V. Lomov, I. Verpoest, Compression of woven reinforcements: a mathematical model, J. Reinf. Plast. Compos. 19 (16) (2000) 1329–1350.
[20] P. Badel, E. Vidal-Sallé, P. Boisse, Large deformation analysis of fibrous materials using rate constitutive equation, Comput. Struct. 86 (11–12) (2008) 1164–1175.
[21] A. Rassineux, 3D mesh adaptation. Optimization of tetrahedral meshes by advancing front technique, Comput. Methods Appl. Mech. Eng. 141 (3–4) (1997) 335–354.
[22] Franco P. Preparata, Michael I. Shamos, Computational Geometry: An Introduction, Springer-Verlag New York, Inc., New York, NY, USA, 1985.
[23] G. Hivet, P. Boisse, Consistent mesoscopic mechanical behaviour model for woven composite reinforcements in biaxial tension, Composites, Part B, Eng. 39 (2) (2008) 345–361.
[24] P. Frey, P.-L. Georges, Mesh Generation, 2nd edition, Wiley–ISTE, ISBN 978-1-84821-029-5, April 2008, 848 pages.

[25] C. Labergère, A. Rassineux, K. Saanouni, Numerical simulation of continuous damage and fracture in metal-forming processes with 2D mesh adaptive methodology, in: 82 Finite Elements in Analysis and Design, 2014, pp. 46–61.
[26] Ch. El Hage, R. Younès, Z. Aboura, M.L. Benzeggagh, M. Zoaeter, Analytical and numerical modeling of mechanical properties of orthogonal 3D CFRP, Compos. Sci. Technol. 69 (1) (2009) 111–116.
[27] H.L. De Cougny, M.S. Shephard, Surface meshing using vertex insertion, in: 5th International Meshing Roundtable, Sandia National Laboratories, October 1996, pp. 243–256.